Energy 307 (2024) 132810

Contents lists available at ScienceDirect

Energy

journal homepage: www.elsevier.com/locate/energy

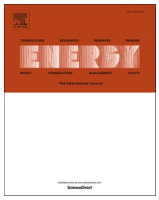

Energy consumption and dilution of toxic gases in underground infrastructures: A case study in a railway tunnel under forced ventilation

Javier Menéndez [a,b], Mariano Sanabria [c], Jesús Manuel Fernández-Oro [d,*], Mónica Galdo-Vega [d], Laura Álvarez de Prado [b], Antonio Bernardo-Sánchez [b]

[a] Sadim Engineering, Oviedo, 33005, Spain
[b] Department of Mining Technology, Topography and Structures, University of León, León, 24071, Spain
[c] Electric Department, Siemens Gamesa, Madrid, 28830, Spain
[d] Fluid Mechanics Department, University of Oviedo, Gijón, 33271, Spain

ARTICLE INFO

Keywords:
Forced ventilation
Tunneling
Toxic gases
Blasting
Re-entry times
Energy consumption
Ventilation ducts

ABSTRACT

Toxic fumes are released after blasting in underground excavations. The analysis of safe re-entry times into the work areas is essential for addressing safety and productivity concerns. In this paper, a railway tunnel 2.1 km long under forced ventilation system is selected as a case study to assess the energy consumption and re-entry times after blasting under different ventilation conditions. First, three-dimensional CFD numerical models were conducted in order to predict the migration time to reduce the levels of noxious gases below the limits established in safety regulations. Field measurements were conducted to verify the accuracy of the results obtained in the simulations. Then, additional analytical models were conducted to evaluate the energy consumed by the ventilation system. The results obtained show that the accumulated re-entry time reaches 414 h for the excavation of the tunnel employing an airflow rate of 40 $m^3\ s^{-1}$. This time increases by 33 % when the airflow rate decreases to 30 $m^3\ s^{-1}$. However, even though the time decreases when the ventilation volume increases, energy consumption increases significantly, reaching 1,306 MWh for a ventilation volume of 40 $m^3\ s^{-1}$ compared to 551 MWh using an airflow of 30 $m^3\ s^{-1}$.

1. Introduction

When utilizing the drilling and blasting method for excavating underground infrastructures, the process results in the generation of toxic gases. Immediate releases after blasting are predominantly composed by nitrogen oxides (NOx) and carbon monoxide (CO) [1]. These noxious gases must be diluted to ensure a safe environment for workers. Therefore, it is crucial to implement an appropriate ventilation system with the correct airflow to reduce the concentrations of hazardous gases to levels below those established in safety regulations. These levels are referred to as threshold limit values (TLVs) and vary depending on each country's regulations [2]. This measure is crucial for maintaining a secure and healthy atmosphere for workers involved in underground construction activities. The safe re-entry time is largely contingent on factors such as the ventilation system in use, the airflow rate and the quantity of explosives employed [3]. In tunneling construction, different ventilation systems can be employed to minimize safe re-entry times after blasting, being the forced ventilation the standard practice. An accurate prediction of these re-entry times into the work areas is thus essential, leading researchers to conduct analyses on the dilution of hazardous gases produced during blasting. Computational Fluid Dynamics (CFD) modeling is a prevalent tool used for this purpose, enabling to predict the evolution and distribution of blasting fumes. Precisely, the dispersion of CO after blasting was investigated in a subsurface mine [3] for different working conditions in a mining tunnel under forcing ventilation systems. It was found that both the distance from the ducting system to the work area as well as the ventilation volume at the end of the duct significantly influence the dispersion coefficient of the noxious gases. Bahrami et al., 2019 [4] conducted a numerical model to assess the re-entry time in a mining infrastructure. The study monitored the return of the ventilation system. The researchers concluded that the monitoring system can serve as a reliable method for determining re-entry times. Torno et al., 2013 [5] employed both conventional and 3D CFD modeling to investigate the evolution of harmful gases in a coal mine. Field measurements were carried out to validate the CFD results, contributing valuable insights into the re-entry

* Corresponding author.
E-mail address: jesusfo@uniovi.es (J.M. Fernández-Oro).

https://doi.org/10.1016/j.energy.2024.132810
Received 28 May 2024; Received in revised form 22 July 2024; Accepted 9 August 2024
Available online 13 August 2024

time for workers returning to the working area. In their numerical analysis, Feng et al., 2022 [6] investigated the dynamic diffusion of CO in a tunnel under forcing mode. The research findings indicated that the duration needed to decrease the concentration of CO increases when the excavation is situated in high-altitude areas.

Other research works focused on underground coal mines have explored the dilution of blasting fumes under secondary ventilation systems [7]. Pu et al., 2020 [8] employed CFD numerical modeling to predict the evolution of blasting fumes in a tunnel. The study considered forcing ventilation and different duct diameters. Additionally, Huang et al., 2015 [9] conducted a research work on the environmental repercussions in tunneling construction. They analyzed the effects of tunnel dimensions employing the drilling and blasting method. Their conclusion highlighted that construction process, mainly the blasting operations, creates hazardous atmospheres, seriously compromising the workers' health.

In efforts to enhance the mining operating cycles, researchers have employed both mathematical and empirical models to predict the dispersion of hazardous gases during blasting [10,11]. Agson Gani et al., 2019 [12] conducted a research work focused on determining re-entry times after blasting in a gold mine. Their analysis encompassed the dispersion of CO, the diffusion coefficient and different ventilation systems. Gas detectors were used to assess the evolution and distribution of harmful gases [13]. A gas monitoring system was used to introduce 1D analytical models to assess the times required to reduce the levels of toxic gases [14]. Furthermore, Harris and Mainiero, 2008 [15] developed a novel approach involving the application of negative pressure to a vertical shaft to eliminate CO levels near the blast. Several researchers have explored the migration of CO and NO after blasting works, examining adverse issues for workers [16,17]. The concentration of harmful gases and dust within the work face is contingent on the layout of forcing ventilation and the chosen tunneling method [18,19]. Li et al., 2016 [20] conducted an examination of air velocity in large subsurface excavations, concluding that air velocities exceeding 0.15 m s^{-1} are essential to effectively minimize CO concentrations below the exposure limits. In a study by Zhang et al., 2016 [21], the migration of CO and dust in mining roadways was investigated, with a notable emphasis on the crucial role of fan selection for an effective removal of the noxious gases generated after blasting. Moreover, underground excavations in high-altitude locations have been explored by several researchers, analyzing the dilution of harmful blasting fumes produced after blasting [22,23]. Their conclusions suggested that at lower altitudes, there is a decrease in the safe re-entry times. Chang et al., 2020 [24] conducted a study that focused on the forcing ventilation system employed during tunneling excavation. Three-dimensional CFD models were developed considering different ducting position, airflow rates and distance from end of the duct to the work area to determine CO concentrations.

Additionally, in tunneling excavation, species transport modeling is employed to investigate the underground environment and dust management considering different ventilation modes. Xin et al., 2021 [25] conducted comparative studies to explore the cooling efficiency in underground excavations. The study considered a tunnel 40 m long equipped with two ducting systems, each having a diameter of 0.8 m. Different lengths of these air ducts were examined within a forced-exhaust ventilation system. The research aimed to assess and compare the effectiveness of different ventilation configurations in maintaining a favorable thermal environment and controlling dust during tunneling activities. Bubbico et al., 2014 [26] conducted a comprehensive CFD analysis to study the evolution of harmful species inside the tunnels, employing k-ε turbulence models. The study focused on examining the generation and management of dust under different conditions. Notably, the researchers concluded that the effective dust management is significantly influenced by the distance from the end of the ducting system to the working area [27,28]. This underscores the critical role of proper ventilation system configuration in mitigating the generation and dispersion of dust during tunneling operations. The time required to reduce the levels of toxic gases has been a subject of study, particularly in a mine, applying the levels of NO_x generated from an ammonium nitrate/fuel oil (ANFO) blast [29]. Understanding the release and dispersion of NO_x is crucial in determining the safety duration for personnel to re-enter the mined area. Presently, monitoring systems of the ventilation return in underground excavations are effectively utilized to determine the time required to dilute the harmful gases below the TLVs [30]. These systems play a pivotal role in assessing the concentration levels of various gases, providing valuable data to ensure the health of workers returning to the post-blast working areas. Adhikari et al., 2022 [31] developed analytical models employing CFD numerical models to investigate the presence of toxic gases in the rock mass and muck pile and their effects on safe re-entry times. They considered a mine development with a ducting system with a length of 35 m long and 1 m in diameter and a muck pile with a volume of 34.2 m^3. De Souza et al., 1993 [32] analyzed the blasting fumes in order to reduce the costs of the ventilation system in underground excavations. CFD models were developed by Nie et al., 2024 [33] to investigate the efficiency of the dust removal systems in underground coal mines. They developed a new type of spiral air curtain generator to improve the pollution control efficiency. The behavior of the dust particles was analyzed by Lu et al., 2022 [34] during underground tunneling. The operation of the rotary cutterhead was simulated using Ansys Fluent and concluded that the increase of the exhaust velocity improves dust suppression.

In this paper, safety and productivity concerns are addressed after blasting operations during underground excavations. A railway tunnel 2.1 km long with a cross-section of 68 m^2 has been selected as a case study to analyze the migration of noxious gases and predict the re-entry times of the workers to the work areas. The migration of toxic gases from blasting has been evaluated in relation to the energy consumption of the ventilation system. Using a novel model, the energy consumption has been obtained after each advance cycle, computing the final consumption for the total excavation length. Three-dimensional CFD and one-dimensional models were conducted considering forced and exhaust ventilation modes with a flexible ducting system 1.8 m in diameter and ventilation volumes of 30 and 40 $m^3 s^{-1}$. Species-transport models were employed to investigate the evolution and distribution of the noxious gases released after blasting. Concentration-time curves of CO, NO and NO_2 are evaluated at different sections of the tunnel in order to determine the time required to reduce the levels of noxious gases below the established TLVs. To verify the accuracy of the results obtained in the numerical simulations, field measurements were carried out when the excavation length reached 200 m. Then, novel 1D analytical models were developed to optimize the re-entry times considering leaky ducting

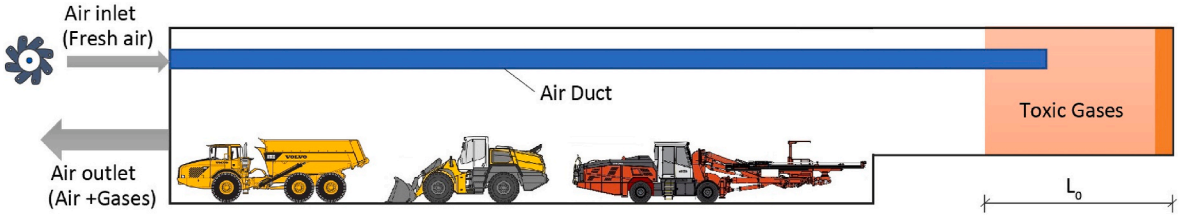

Fig. 1. Section of the railway tunnel. Mobile equipment, ventilation system and noxious gases concentrate on the tunnel face.

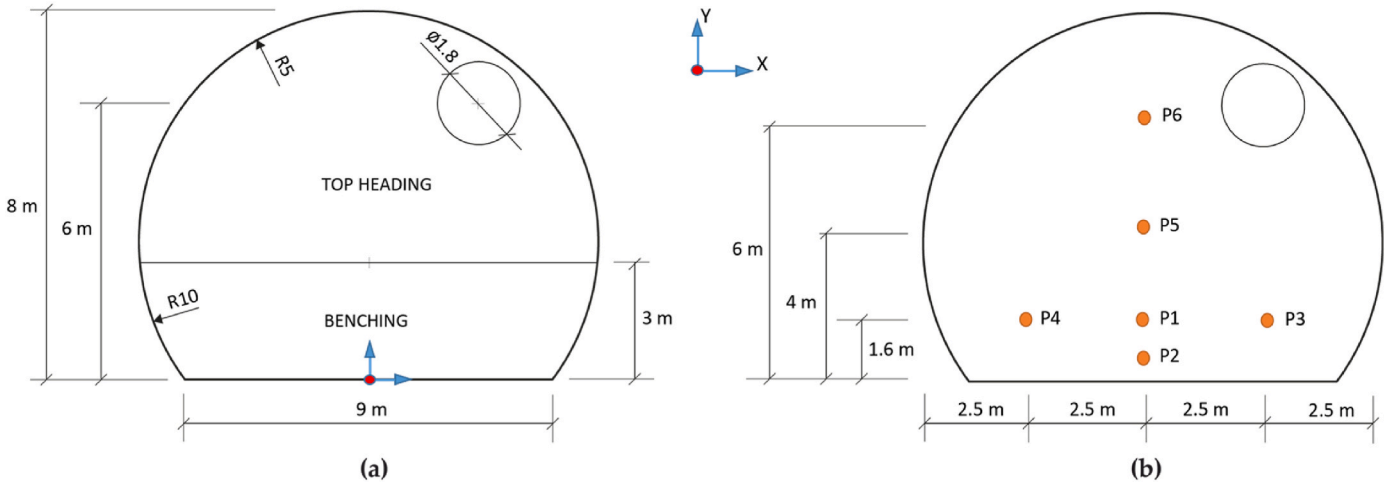

Fig. 2. Cross-section of the tunnel. (a) Top heading, benching and ventilation duct; (b) Location of observation points in the full face of the tunnel.

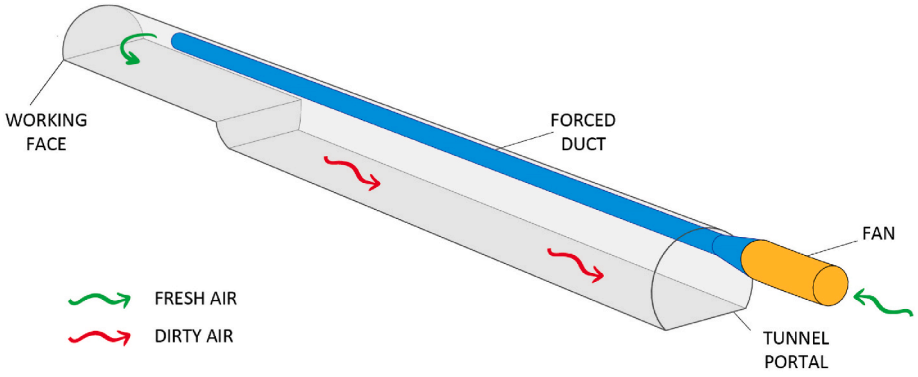

Fig. 3. Typical forced ventilation scheme in a tunnel. Axial fan located at the tunnel portal and flexible ventilation duct from the tunnel portal to the working area.

systems. Pressure drops and air leaks along the ventilation ducts were investigated and the power of the fan was calculated for the two airflow rates used. Therefore, the energy consumed by the ventilation system during the total excavation length was evaluated and compared for both ventilation volumes. Additionally, the total accumulated re-entry time for tunnel excavation was also estimated for both scenarios. Finally, in order to optimize the construction process and reduce the production delays, a balance is performed between the reduction in re-entry time and the potential increase in energy consumption.

2. Methodology

2.1. Problem statement

During the excavation of underground infrastructures using the drilling and blasting method, forced ventilation systems are commonly employed. These systems play a crucial role in managing air quality and mitigating the release and dispersion of toxic gases generated during the blasting process. Fig. 1 shows the longitudinal section of the tunnel. The fresh air reaches the work area through the flexible ducting system. The main mobile equipped used, dumper truck, loader and jumbo, as well as the air duct, are also presented in Fig. 1. The air volume must be properly designed to guarantee the safety of the construction workers. The air volume is determined depending on the power of diesel engines and number of workers. Harmful gases, mainly CO and NO_x, are released immediately after blasting works. Construction operations inside the tunnel must be interrupted until gas concentrations are reduced below established TLVs according to the safety regulations. The time that passes from blasting until the gases reach safe values is known as safe re-entry time. As presented in Fig. 1, immediately after blasting, the gases concentrate in the vicinity of the tunnel face, occupying a tunnel length L_0. This throwing length of the noxious gases (L_0) can be calculated depending on the quantity of explosives (kg) used in the blasting.

Fig. 2 shows the cross-section of the railway tunnel considered as a case study. The cross-section of the tunnel is 68 m^2. The full section has a height of 8 m and a width of 9 m, while the top heading, excavated in the first phase, is 5 m high and 10 m width (39 m^2). A flexible ventilation ducting system 1.8 m in diameter is considered (duct axis X = 2.5 m, Y = 6 m). The duct is located on the right haunch at a height of 6 m. Six observation points located as indicated in Fig. 2b are considered to investigate the toxic gases concentration produced after blasting in different areas of the section.

The scheme of the forcing ventilation mode is illustrated in Fig. 3. The ventilation volume provided by the fan reaches the heading face through the flexible duct. The dirty air (dust and toxic gases from blasting and combustion equipment) returns towards the tunnel exit (Z = 0 m) through the tunnel section. According to the number of workers and power of diesel engines operating simultaneously, airflow rates at the working face of 30 and 40 $m^3\ s^{-1}$ are considered. The airflow rates also consider the minimum cross-section wind speed.

2.2. Concentration of toxic gases and threshold limit values

CO and NO_x are mainly released after blasting during the tunnel excavation. The throwing length of the harmful gases in the working face after blasting (L_0) can be determined by applying Eq. (1) depending

Table 1
TLVs for CO, NO and NO_2 [7,39].

Gas	TWA (ppm)	STEL (ppm)
CO	25	100
NO	25	30
NO_2	3	5

on the quantity of explosives (G) [3,35,36]. The initial concentration of the harmful gases (C_0) can be obtained by applying Eq. (2), where G is the amount of explosives used (kg), M_{GAS} and M_{AIR} are the molar mass of gas and air, respectively, (g mol^{-1}), L_0 is the initial throwing length of gases, A is the cross section of the tunnel (top heading), b is the ratio of toxic gas ($m^3\ kg^{-1}$) and depends on the type of explosives. According to the type of explosives used (emulsion), a gas volume of 0.014, 0.00125 and 0.00065 $m^3\ kg^{-1}$ of CO, NO and NO_2, respectively, were considered [37–39]. The TLVs considered, time weighted average (TWA) and short-term exposure limits (STEL), are depicted in Table 1 for CO, NO and NO_2. TWA represents the highest average concentration of an airborne substance, measured over the duration of an 8-h workday and five-day working week. STEL refers to the maximum concentration of a substance in the air, as a time-weighted average over a 15-min period.

$$L_0 = 15 + \frac{G}{5} \tag{1}$$

$$C_0 = \frac{G\ b\ M_{GAS}}{L_0\ A\ M_{AIR}} \tag{2}$$

2.3. CFD numerical modeling

2.3.1. Mathematical models

Numerical simulations using 3D CFD numerical modeling have been developed to investigate the migration of harmful gases following blasting operations. This sophisticated modeling approach allows for a detailed simulation and analysis of how these gases disperse in the environment after blasting, providing valuable insights into their behavior and potential impact. Ansys Fluent software has been employed to resolve the 3-D Unsteady URANS equations. The transient species transport model was selected considering the realizable k-ε turbulence model [40]. In addition, the PISO algorithm has been employed to model the coupling between pressure and velocity during the iterative procedure. A time step of 0.1 s was set to reach the solution convergence. Reynolds-averaged Navier-Stokes (RANS) Eqs. (3) and (4) are used to simulate the phenomena of interest. The RANS equations are a set of time-averaged fluid flow equations that can be used to model turbulent flow in CFD problems.

$$\frac{\partial \rho}{\partial t} + \frac{\partial}{\partial t}(\rho u_i) = 0 \tag{3}$$

$$\frac{\partial}{\partial t}(\rho u_i) + \frac{\partial}{\partial x_i}(\rho u_i u_j) = \frac{\partial p}{\partial x_i} + \frac{\partial}{\partial x_j}\left[\mu\left(\frac{\partial u_i}{\partial x_j} + \frac{\partial u_j}{\partial x_i} - \frac{2}{3}\delta_{ij}\frac{\partial u_l}{\partial x_l}\right)\right] + \frac{\partial}{\partial x_j}\left(-\rho\overline{u_i' u_j'}\right) \tag{4}$$

RANS equations have the same general form as the instantaneous Navier-Stokes equations, but the velocity and other solutions represent time-averaged values. The RANS equations contain an additional Reynolds stress term $-\rho\overline{u_i' u_j'}$ that must be modelled to close the system of equations. Realizable k-ε turbulence model is used to model the Reynolds stresses and close the momentum Eq. (4). The realizable k-ε model is a two-equation turbulence model that solves two separate transport equations to determine the turbulent velocity and length scales independently. The two transport equations in the realizable k-ε model are for the turbulent kinetic energy (k) (5) and its dissipation rate (ε) (6). The k equation represents the kinetic energy per unit mass in the turbulent fluctuations, while the ε equation models the rate of dissipation of the turbulent kinetic energy.

Table 2
Setting values of the CFD model.

Property	Setting
Model	3D-URANS Unsteady
Species	Transport model with diffusion energy sources
Materials	Air, CO, NO, NO_2
Pressure velocity Coupling	PISO
Turbulence model	Realizable k-ε
Transient Coefficients	Time step 0.1 s
Convergence Criterion	10E-5
Intel Boundary Condition	Velocity Inlet
Outlet Boundary Condition	Pressure outlet

$$\frac{\partial}{\partial t}(\rho k) + \frac{\partial}{\partial x_j}(\rho k u_j) = \frac{\partial}{\partial x_j}\left[\left(\mu + \frac{\mu_t}{\sigma_k}\right)\frac{\partial k}{\partial x_j}\right] + G_k + G_b - \rho\varepsilon - Y_M + S_k \tag{5}$$

$$\frac{\partial}{\partial t}(\rho \varepsilon) + \frac{\partial}{\partial x_j}(\rho \varepsilon u_j) = \frac{\partial}{\partial x_j}\left[\left(\mu + \frac{\mu_t}{\sigma_\varepsilon}\right)\frac{\partial \varepsilon}{\partial x_j}\right] + \rho C_1 S_\varepsilon - \rho C_2 \frac{\varepsilon^2}{k + \sqrt{\upsilon\varepsilon}} + C_{1\varepsilon}\frac{\varepsilon}{k}C_{3\varepsilon}G_b + S_\varepsilon \tag{6}$$

In addition, the convection-diffusion Eq. (7) is used to predict the local mass fraction of each species.

$$\frac{\partial}{\partial t}(\rho Y_i) + \frac{\partial}{\partial x_i}(\rho u_i Y_i) = -\nabla \cdot \vec{J_i} + R_i + S_i \tag{7}$$

The first term on the left-hand side represents the rate of change of species mass fraction, while the second term represents the convective transport of species by the fluid flow. The terms on the right-hand side account for diffusive transport $\vec{J_i}$, chemical reaction R_i, and addition from the dispersed phase S_i .In turbulent flows, the diffusion flux $\vec{J_i}$ is modelled using the gradient diffusion hypothesis, which relates the diffusion flux to the gradient of the mean species mass fraction according to Eq. (8).

$$\vec{J_i} = -\left(\rho D_{i,m} + \frac{\mu_t}{Sc_t}\right)\nabla Y_i - D_{T,i}\frac{\nabla T}{T} \tag{8}$$

where $D_{i,m}$ is the molecular diffusion coefficient and $D_{T,i}$ is the turbulent diffusion coefficient, which is typically modelled using a turbulence model. In the k-ε realizable model Sc_t represents the turbulent Schmidt number $\frac{\mu_t}{\rho D_t}$ where μ_t is the turbulent viscosity. The setting values of the CFD models are presented in Table 2.

2.3.2. Mesh and boundary conditions

A railway tunnel, spanning a length of 200 m and featuring a cross-section of 68 m^2, was considered. A total of 1.84 M of hexahedral elements were used to mesh the total geometry of the tunnel and ventilation duct. The model geometry and the detail of the mesh grid are depicted in Fig. 4. A view of the tunnel portal and duct inlet is presented in Fig. 4a. A detail of two cross-sections and the ventilation duct are presented in Fig. 4b.

The detail of the cross-sectional areas considered for the railway tunnel to investigate the concentration-time curves and the boundary conditions are shown in Fig. 5. According to the throwing length of the harmful gases in the drilling face immediately after blasting, the gas was considered as a mixture of CO and NO_x at atmospheric conditions. The noxious gases concentrations immediately after blasting has been considered as a boundary condition and obtained by applying Eq. (2). The concentrations of the CO, NO and NO_2 are indicated in Table 3. It is assumed that the concentration of noxious gases is uniformly distributed in the throwing area (L_0) immediately after blasting. In addition, the velocity inlet at the duct outlet was also selected as a boundary condition depending on the air volume at the heading face considered, 30 or 40 $m^3\ s^{-1}$. The boundary conditions, initial volume of noxious gases,

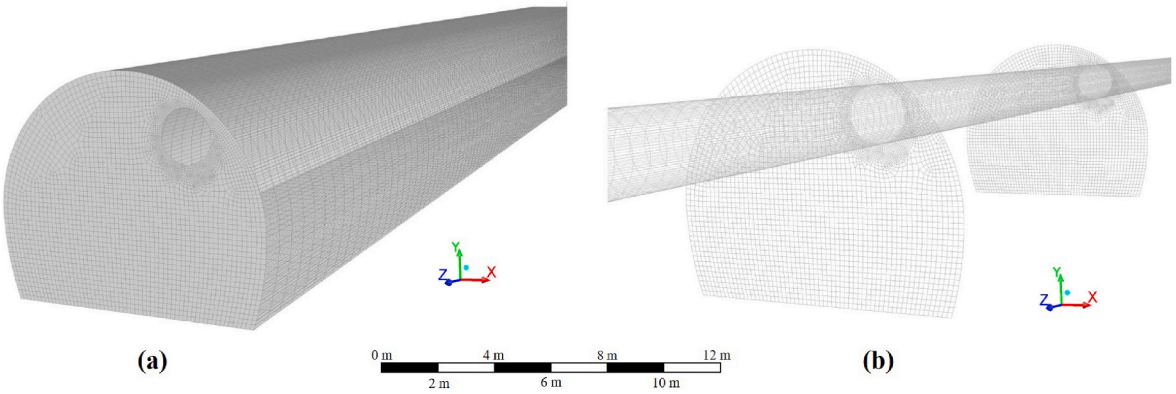

Fig. 4. Model geometry and mesh grid. (a) Detail of the tunnel portal; (b) Cross sections and ventilation duct.

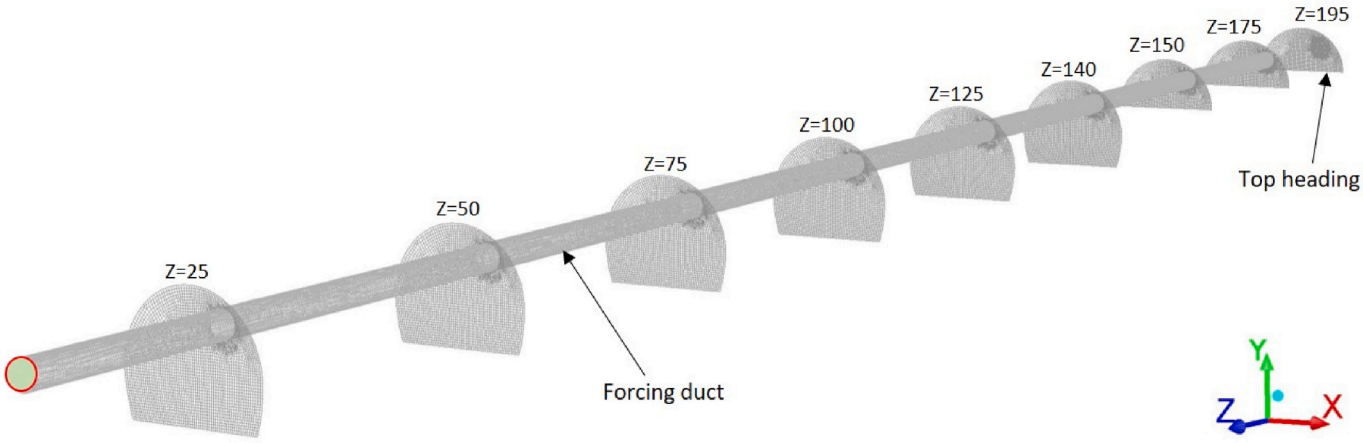

Fig. 5. Tunnel sections every 25 m long, from Z = 25 to Z = 195 m.

Table 3
Concentrations of CO, NO and NO_2.

Gas	C_0 (ppm)
CO	1053.74
NO	100.80
NO_2	80.54

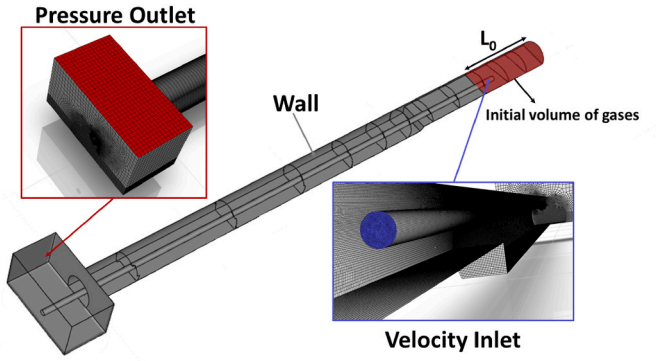

Fig. 6. Boundary conditions.

velocity inlet and pressure outlet, are shown in Fig. 6.

2.3.3. Grid sensitivity and time step independence analysis

Three different mesh models were used to analyze the grid sensitivity analysis: coarse, medium and fine mesh sizes. A number of elements of 1.45 M, 1.84 M and 2.23 M were considered for the coarse, medium and fine models, respectively. The analysis focused on the CO concentration after blasting at Z = 150 (full section), applying an air volume at the heading face of 40 $m^3\ s^{-1}$. The CO concentration-time curve is presented if Fig. 7a for the tunnel section Z = 150 m. The medium size grid model with 1.84 M of elements was finally used to optimize the efficiency and computing cost during the simulations.

A time step independence study was carried out considering time steps of 0.5, 0.1 and 0.05 s. The NO_2 concentration-time curve was simulated at Z = 100 m using an air volume of 30 $m^3\ s^{-1}$. According to the results depicted in Fig. 7b, the time step size has a reduced effect on the results. Therefore, a time step of 0.1 was selected in the 3D CFD simulations.

2.4. Analytical models

In the present investigation, two analytical models have been employed sequentially to obtain a tight estimation of the energy consumption of the ventilation system required during the excavation of a railway tunnel to ensure safety work conditions. To mimic real working operations, the tunnel length is progressively enlarged, so the models are executed recursively to accommodate a tunnel advance rate of 5.4 m

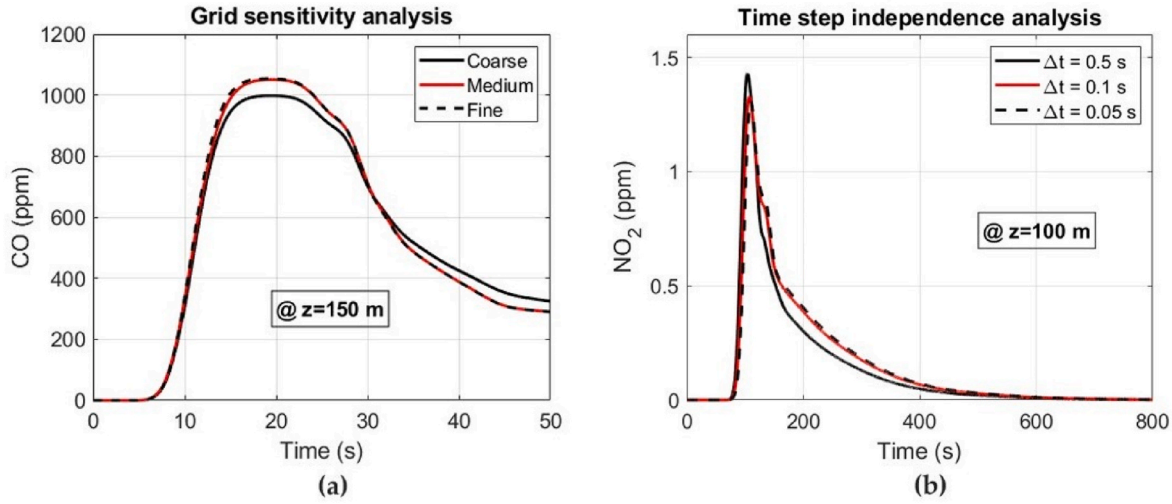

Fig. 7. (a) Grid sensitivity analysis. CO concentration-time curve at section Z = 150 m considering a ventilation volume of 40 $m^3\ s^{-1}$; (b) Time step size independence study. NO_2 concentrations at Z = 100 m considering a ventilation volume of 30 $m^3\ s^{-1}$.

day^{-1}, thus resulting in a one-dimensional tunnel increasing in length up to a final distance of 2.1 km. The blasting parameters employed for every advancement is considered in the model as an initial amount of toxic gases (CO, NO and NO_2), accumulated in the drilling face, that needs to be ventilated for the workers to initiate a new operating cycle.

2.4.1. One-dimensional model for gas dispersion after blasting

A previously developed model by the authors to compute the turbulent transport and molecular diffusion of toxic gases within a tunnel section has been resolved numerically in MATLAB. A one-dimensional model has been developed considering a third-order QUICK scheme to analyze convective terms [38]. As shown in preliminary test, the explicit approach is accurate for the temporal term. To assure sufficient stability and convergence, a variable time step has been applied to keep both Courant number and diffusion number below 0.1 and 0.05 respectively as the length of the tunnel was progressively increased. A mesh size of $\Delta x = 1$ m has been adopted for the longitudinal section in the tunnel. The basic transport equation for gas concentration C in the tunnel has been resolved as given in Eq. (9), while the effective diffusion coefficient D in the transport equation has been estimated using Eq. (10), based on the friction factor f computed in Eq. (11). S_c is a term source of generation or destruction of gas concentration in some area of the tunnel. Finally, the hydraulic diameter (D_H) is computed by applying Eq. (12), A is the tunnel area (m^2) and *per* is the tunnel perimeter (m).

$$\frac{\partial C}{\partial t} + \overline{u}\frac{\partial C}{\partial x} = D\frac{\partial^2 C}{\partial x^2} + S_c \tag{9}$$

$$D = 5.05\, D_H\, \overline{u}\sqrt{\frac{f}{8}} \tag{10}$$

$$\frac{1}{\sqrt{f}} = 2\ log_{10}\left(\frac{D_H}{2\varepsilon}\right) + 1.74 \tag{11}$$

$$D_H = \frac{4A}{per} \tag{12}$$

A typical value of roughness in tunnels, $\varepsilon = 0.015\ m$ has been adopted [41], resulting in a friction factor value of $f = 0.023$. For the analytical approach, the duct area (1.8 m in diameter) is subtracted from the practical area of the full face (68 m^2), and a uniform air flow velocity $\overline{u}$ is simply adopted as the ratio of the air volume and the cross-section of the tunnel for the convective terms. However, to simulate the complex three-dimensionality of the flow (especially in the dead end of the tunnel), a longitudinal velocity variation has been finally implemented -going from zero velocity to the maximum bulk flow-to consider the initial reverse flow conditions. To analyze the whole excavation process, this 1D dispersion model has been executed repeatedly to consider the actual length of the tunnel, starting from zero (tunnel portal) up to the final extension of 2.1 km, using a typical excavation rate of 5.4 m day^{-1}. For every update of the tunnel length, the time required for the gas concentration to reach a given minimum TLV is computed and accumulated in order to estimate the total re-entry time required to fulfill clean ambient conditions during the construction of the 2.1 km of the tunnel. The TLVs (TWA and STEL) considered in the simulations are shown previously in Table 1.

Table 4
Ducting classes according to the Standard SIA 196 [42,43].

Ducting Quality	Friction coefficient, λ (–)	Leakage surface, f` ($mm^2\ m^{-2}$)
S	0.015	5
A	0.018	10
B	0.024	20

2.4.2. One-dimensional model for air leakage in the ventilation duct

The operating ventilation rate in the tunnel is provided by a ventilation system composed typically by a flexible leaky duct and an axial fan equipped with a variable frequency drive [42]. However, due to the difficult operative conditions, the ducts are susceptible of suffering damage leading to leakages and flow losses. In addition, air leaks also occur at the joints between the different duct segments. International Standards allow to estimate those air leaks as a function of the material maintenance, classifying ventilation ducts as S, A or B classes [43]. The main parameters of the vent ducts, friction coefficient and active leakage surface, are shown in Table 4 for the three duct classes considered. The fan power required to overcome these losses can be then modelled depending on the duct class and length (i.e., the tunnel length) and the rest operative parameters.

For that purpose, an additional one-dimensional model has been employed to calculate the required total inlet pressure for the fan in order to ensure a net ventilation volume into the work area. Fig. 8 shows a typical scheme of leaky ducts with a length L employed in tunnel ventilation systems. The air volume in the heading face (Q_w) is lower than the air volume at the fan outlet (Q_f) when leaky ducting systems are employed in tunneling ventilation. Therefore, the air leakage flow rate must be analyzed in order to ensure the needed airflow rate in the working area. The airflow rate in the tunnel face area (Q_w) can be

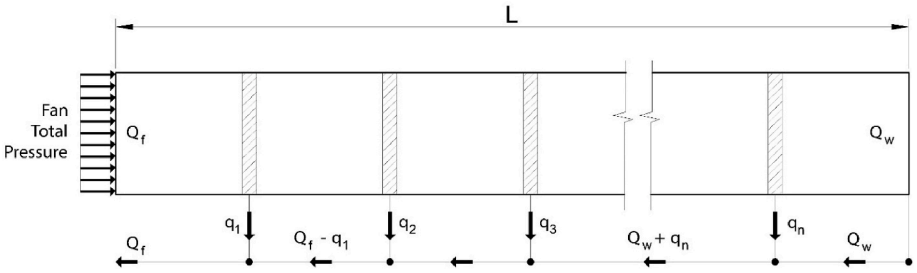

Fig. 8. Air leakage scheme in forced ventilation ducts.

Fig. 9. Field measurements in a railway tunnel. (a) Location of flexible vent duct in the full section; (b) Top heading.

obtained by applying Eq. (13).

$$Q_w = Q_f - \sum_{i=1}^{n} q_i \tag{13}$$

A 1D equations system defined by Eq. (14) and Eq. (15) was developed to determine the pressure drop as well as the air leakage along the ducting (q_i) and the air velocity along the forded ducts considering the three duct classes. The fan output power can be obtained by applying Eq. (16).

$$\frac{du}{dx} = \frac{4f'}{d}\sqrt{\frac{2p}{\rho(1+\zeta)}} \tag{14}$$

$$\frac{dp}{dx} = \frac{\lambda}{d}\rho\frac{u^2}{2} \tag{15}$$

$$P = \frac{p_T\, Q_f}{\eta} \tag{16}$$

where u is the air velocity inside the ventilation duct (m s^{-1}), d is the diameter of the ducting system (m), λ is the characteristic friction factor (−), and p represents the evolution of the static pressure along the ducting system. Additionally, f' represents a leakage parameter, whereas ζ holds for a coefficient of minor losses, typically around 0.3 [40], P is the fan power (W), p_T is the total pressure (Pa), Q_f is the ventilation volume at the fan outlet (m^3 s^{-1}) and η is the fan efficiency (%).

To achieve the required ventilation volume at the mouth of the vent duct (Qw), the fourth-order Runge-Kutta method was systematically applying MATLAB code to solve the equations system, so the distribution of leakage flows, q_i, in the scheme shown in Fig. 7 and Eq. (13) could be determined. Note that this numerical routine required of an iterative process to retrieve the impulsion flow rate of the fan to ensure the desired net flow rate at the work area. A convergence threshold of 10^{-3} was established, requiring approximately 10,000 iterations to reach the final solution, especially in challenging scenarios (such as a representative situation with n = 10 leakage points). The model calculates pressure and velocity distributions, denoted as $p(x)$ and $u(x)$, respectively, along the ventilation duct as functions of the number of leakage points. This iterative process is crucial for obtaining accurate and reliable results in the simulation, particularly when dealing with complex conditions like multiple leakage points, which are equally spaced throughout the system. Note again that these computations must be revisited as the tunnel length is continuously enlarged according to the previous sub-model, thus allowing to calculate the actual fan power required as a function of the present tunnel length. A fully tight estimation of the overall energy consumption required to complete the

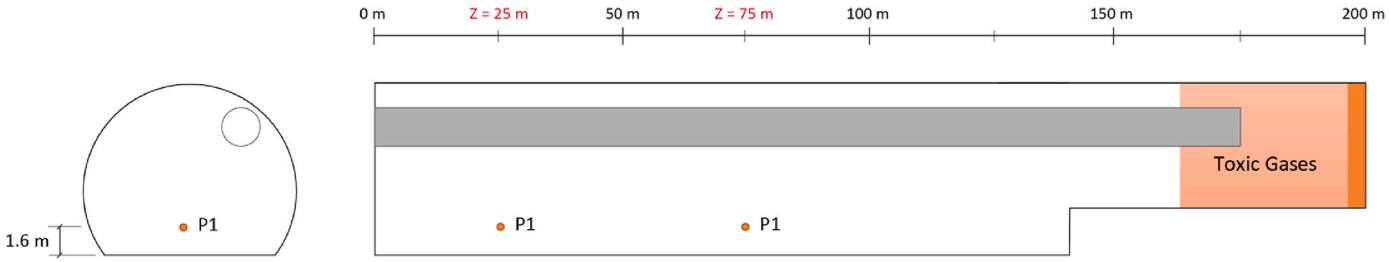

Fig. 10. Measuring points at Y = 1.6 m and Z = 25, Z = 75 m.

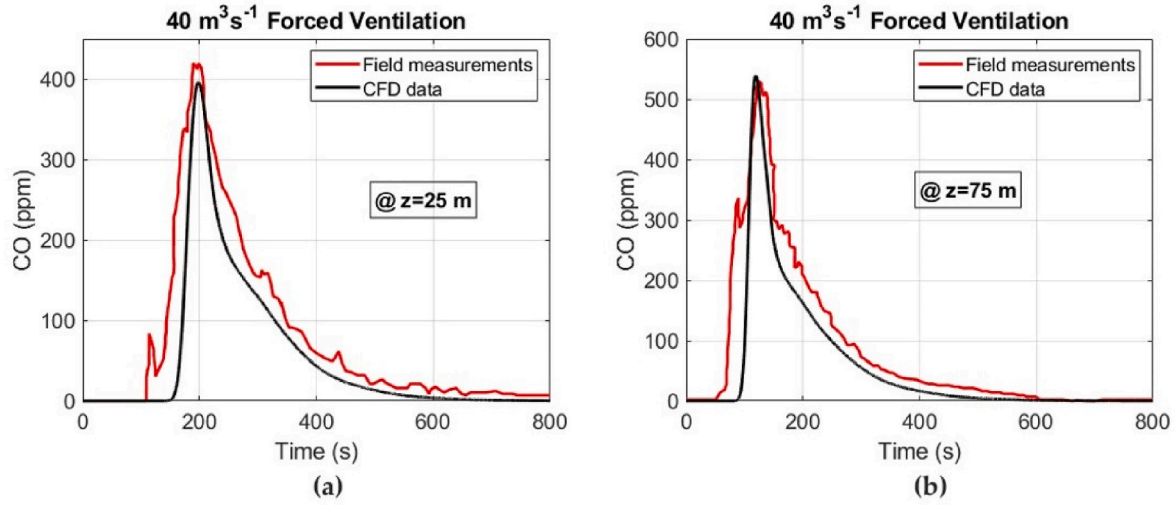

Fig. 11. Field measurements and CFD data. (a) CO concentration at Z = 25 m; (b) CO concentration at Z = 75 m.

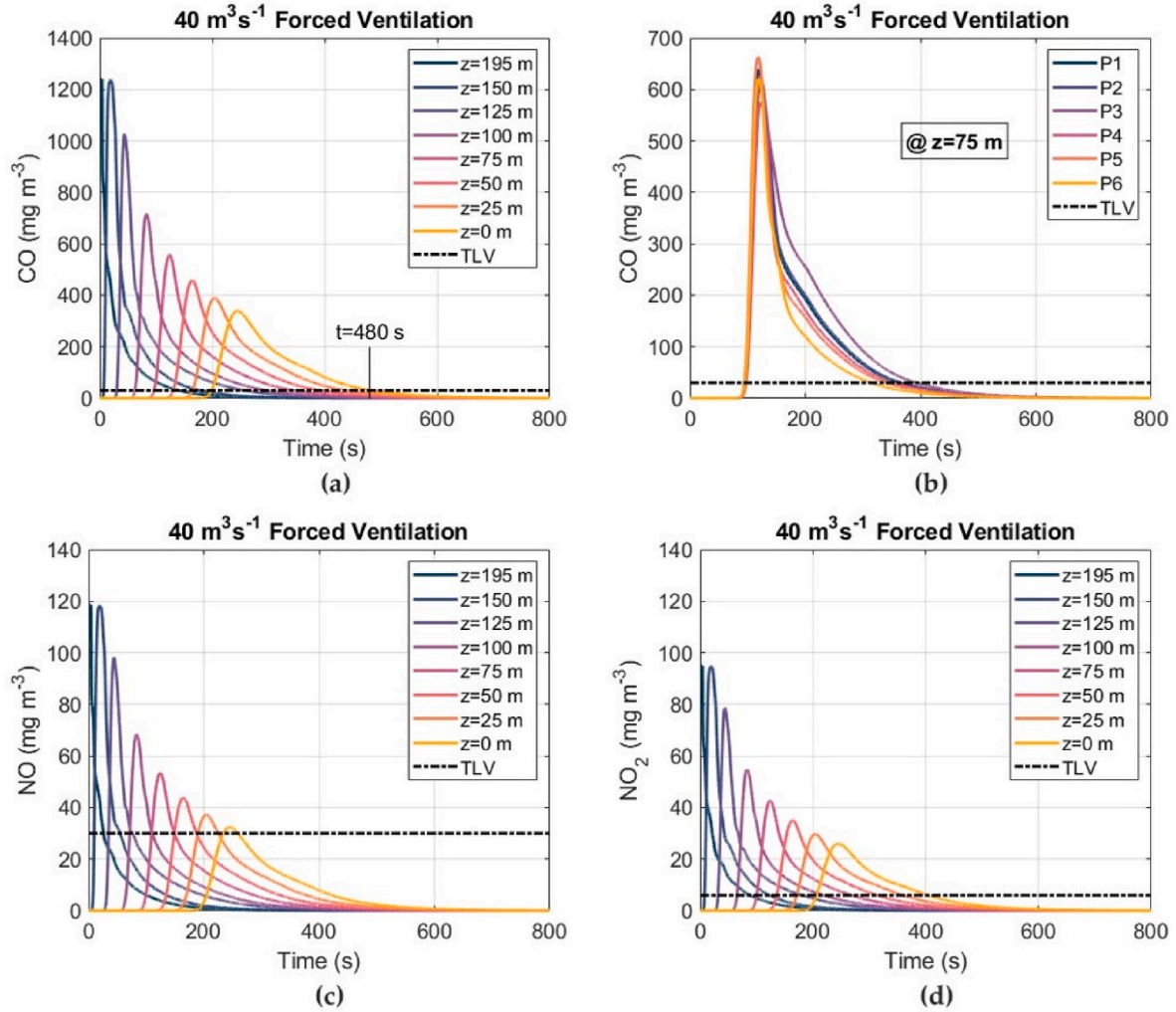

Fig. 12. CDF results. Concentration-time curves of noxious gases at different sections along the tunnel considering a ventilation volume of 40 m^3 s^{-1}. (a) Concentration of CO; (b) Concentration of CO in the observation points at Z = 75 m; (c) Concentration of NO; (d) Concentration of NO_2.

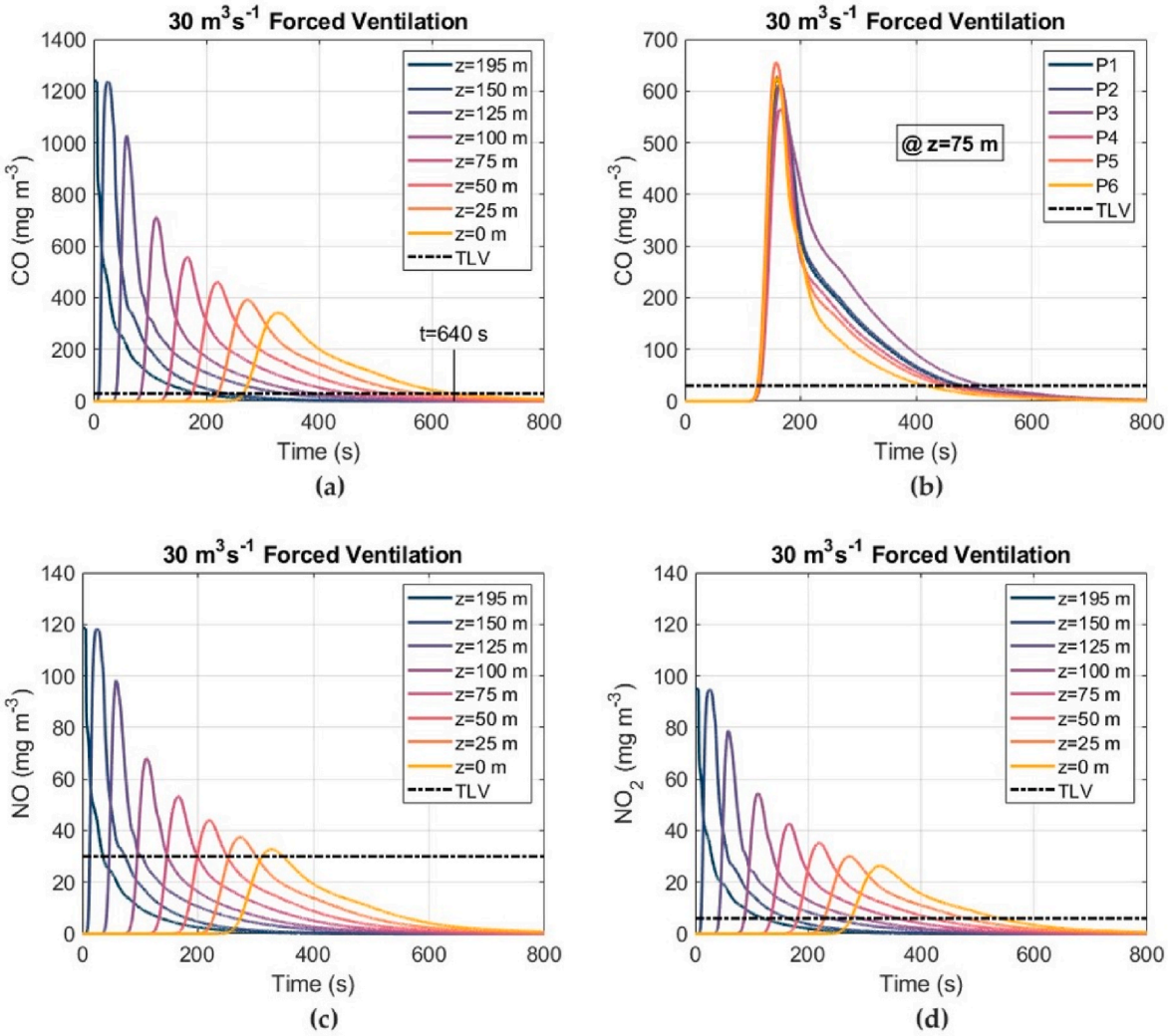

Fig. 13. CDF results. Concentration-time curves of noxious gases at different sections along the tunnel considering a ventilation volume of 30 m^3 s^{-1}. (a) Concentration of CO; (b) Concentration of CO in the observation points at Z = 75 m; (c) Concentration of NO; (d) Concentration of NO_2.

excavation of the tunnel can be then obtained through the accumulated number of energy consumptions for every tunnel advancement.

2.5. Model validation

In order to verify the precision of the CFD results, practical measurements of the CO concentrations were conducted during the construction works when the tunnel reached 200 m long, as illustrated in Fig. 9. Fig. 9a shows the full section with the flexible ducting system. As considered in the CFD model, the construction method used to excavate the tunnel was top heading and benching. A volume of fresh air of 40 m^3 s^{-1} was used at the end of the ducting system under forcing ventilation mode. The blasting parameters (type and quantity of explosives) used during the blasting operations are those that were considered in the CFD modeling. Emulsion explosives were utilized for excavating the primary heading (Fig. 9b). A fan 250 kW power, including a frequency inverter and a PVC ventilation duct 1.8 m in diameter, were employed. The end of the forced duct was positioned at 25 m from the working area (Z = 175 m). Field measurements were conducted utilizing conventional sensors (TROLEX TX 9165), which has a CO range of 0–1000 ppm. The measurements were taken at a height of 1.6 m in two specific sections, Z = 25 and Z = 75 m. The specific locations of the measuring points are illustrated in Fig. 10.

Fig. 11 depicts a comparison between CFD results and field measurements for the concentrations CO at Z = 25 m and Z = 75 m employing an air volume of 40 m^3 s^{-1}. The results reveal an excellent agreement between CFD data and field measurements values at the operating conditions considered. An error range of 3.34 % and 4.36 % between the field measurements and the CFD results has been obtained at Z = 25 m and Z = 75 m, respectively. This underscores the proficiency of the conducted numerical model in accurately forecasting the dispersion of toxic gases released immediately after blasting works and dependably determining safe re-entry times.

3. Results and discussion

3.1. CFD results

The simulations were conducted when the tunnel excavation reached a length of 200 m. The evolution of the gases concentration over time is shown in Fig. 12 using a ventilation volume of 40 m^3 s^{-1}. The instant t = 0 s coincides with the start-up of the ventilation system after blasting, being the instant at which the gas dilution process begins. The concentrations were analyzed at different sections along the tunnel, from the tunnel face to the tunnel portal. As illustrated in Fig. 12, the concentrations profiles for the toxic gases exhibit an inverse-gamma like distribution, characterized by a rapid growth and a subsequent slower decrease. Fig. 11a depicts the distribution of the CO concentrations at

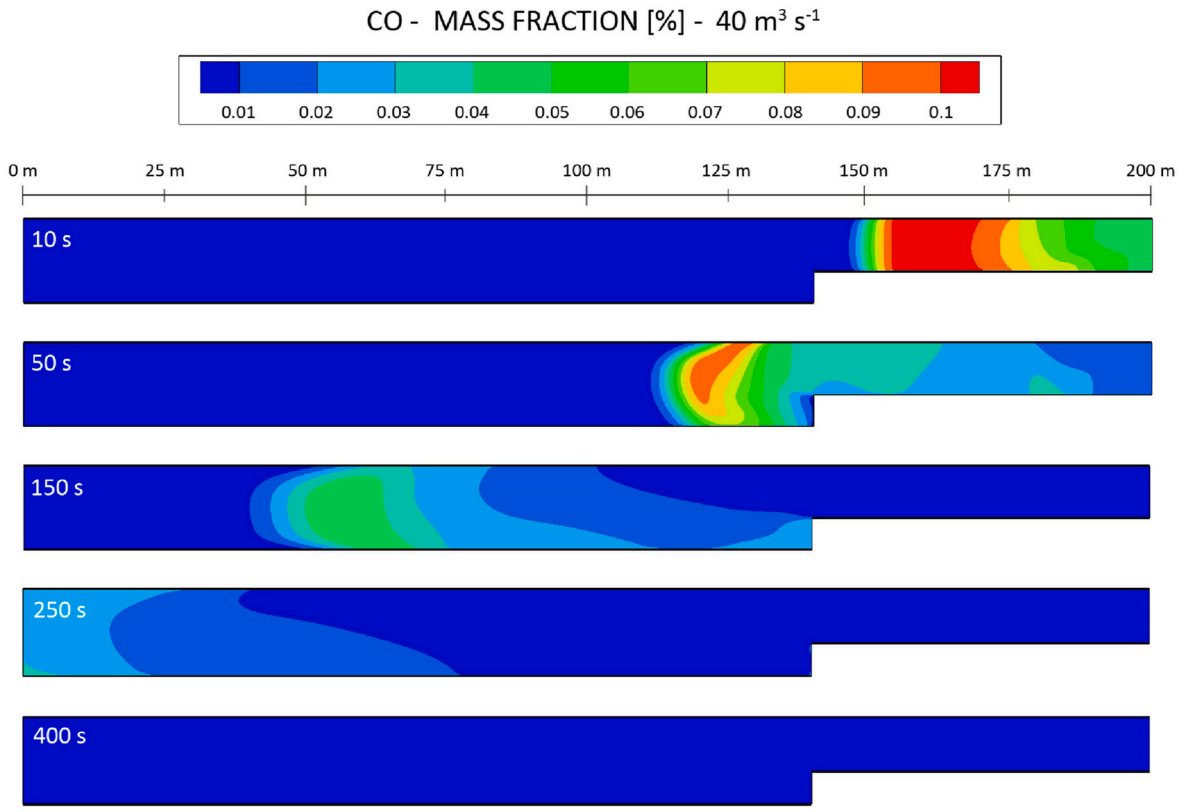

Fig. 14. Evolution of the CO concentration along the tunnel length at different times after blasting considering a ventilation volume of 40 m^3 s^{-1}.

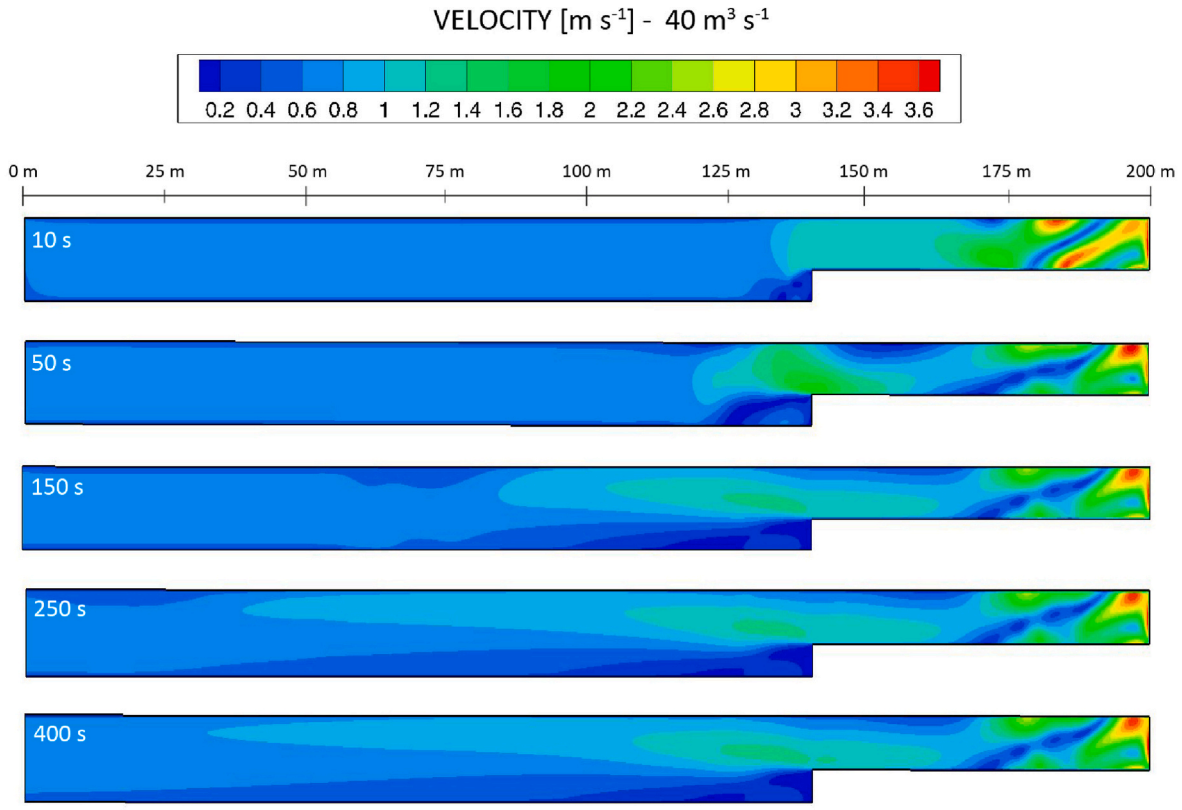

Fig. 15. Velocity profile along the tunnel (X = 0 m) at different times considering a ventilation volume of 40 m^3 s^{-1}.

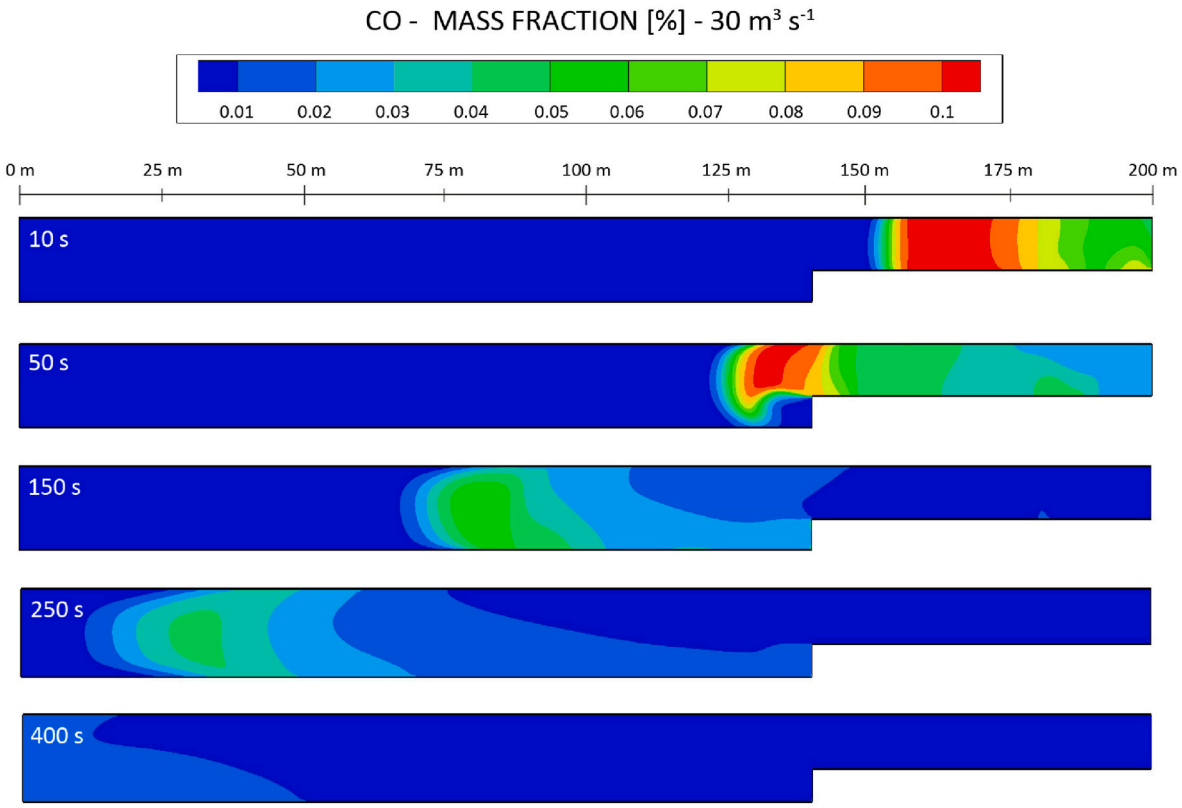

Fig. 16. Evolution of the CO concentration along the tunnel length at different times after blasting considering a ventilation volume of 30 m^3 s^{-1}.

different tunnel sections with a TLV of 25 ppm according to the values showed in Table 1. The concentrations of NO and NO_2 after blasting are shown in Fig. 12c and d, respectively, with their respective TLVs. The concentration peaks reached in different cross-sections decrease as the fume plug progresses towards the tunnel portal. The results obtained confirm that CO is the critical gas, requiring more time to reduce its concentration to levels below those established in the TLVs according to the regulations. The time elapsed from the end of the blasting until the CO concentration drops below 25 ppm reaches 480 s. As seen in Fig. 12c and d, the times to reduce the concentrations of NO and NO_2 below the exposure limits are lower.

Fig. 13 presents the evolution of the concentration of noxious gases using a ventilation volume at the end of the ducting system of 30 m^3 s^{-1}. The CO concentration reaches levels below 25 ppm after 640 s from the blasting, increasing the re-entry time into the work area compared to the previous scenario. Fig. 12b shows the curve of concentration-time for CO at section Z = 75 m at different points of the section. The CO concentration peak experiences a delay compared to the scenario considering a ventilation volume of 40 m^3 s^{-1} (Fig. 12b). All points exhibit identical behavior in the growth phase, with small differences in peak values. However, the evolution of the concentration varies at different points in the tunnel section during the slow decline phase, with a higher concentration of CO at point P3, located beneath the vent duct, and lower levels at point P6.

As has been seen in the results obtained in the CFD model, validated with field measurements, the evolution of the CO concentration is essential to determine the re-entry times into the works area after blasting. Fig. 14 shows the evolution of the CO concentration (%) along the tunnel, from the tunnel portal (Z = 0 m) to the drilling face (Z = 200 m), using a ventilation volume of 40 m^3 s^{-1} when the excavation length reaches 200 m. The CO distribution is presented for different times after blasting, t = 10, t = 50, t = 150, t = 250 and t = 400 s. The forced ventilation system moves the gases towards the exit of the tunnel, decreasing its concentration as the plug approaches the tunnel portal.

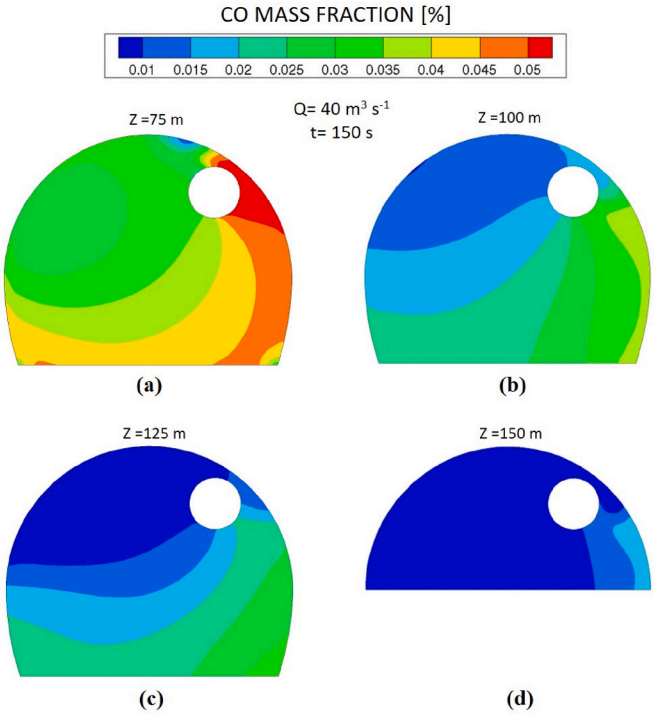

Fig. 17. Distribution of CO concentrations in different sections at t = 150 s using a ventilation volume of 40 m^3 s^{-1}. (a) Z = 75 m; (b) Z = 100 m; (c) Z = 125 m; (d) Z = 150 m.

The velocity profile along the tunnel axis (X = 0 m) is shown in Fig. 15 during the entire process after blasting. Significant changes are observed in the evolution of flow velocity as the toxic gases are diluted and

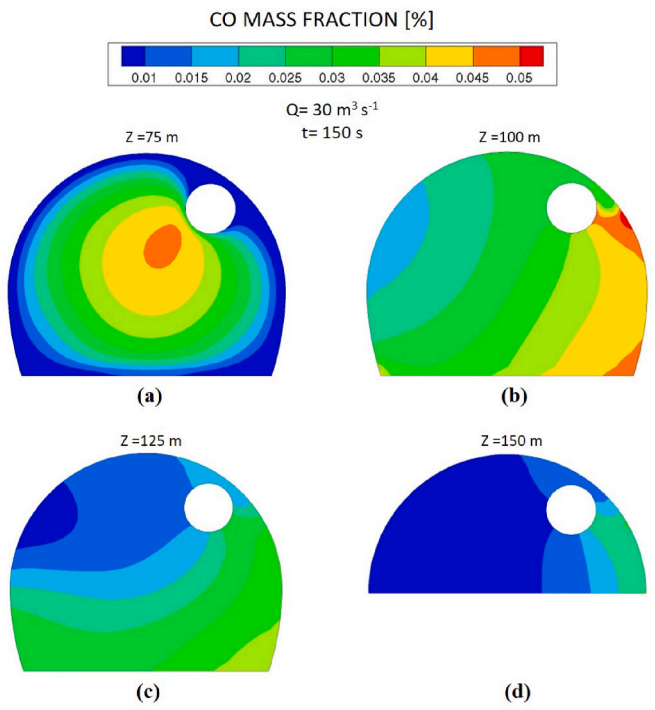

Fig. 18. Distribution of CO concentrations in different tunnel sections at t = 150 s using a ventilation volume of 30 m^3 s^{-1}. (a) Z = 75 m; (b) Z = 100 m; (c) Z = 125 m; (d) Z = 150 m.

displaced towards the exit. This will have a significant impact on the advection of toxic gases concentration, retarding the air renewal and enlarging the safety time lapse between advance cycles. Therefore, this effect should be introduced somehow in 1D dispersion models to achieve more accurate predictions. The velocity distribution can be compared with the evolution of the CO mass fraction presented in Fig. 14. High speeds are observed in the vicinity of the tunnel face, where the discharge of airflow occurs from the ventilation duct. The air velocity reaches 15.7 m s^{-1} at the duct outlet, impacting the tunnel face and recirculating towards the mouth of the ducting, forming a vortex zone in the working area.

Likewise, the evolution of the CO mass fraction is depicted in Fig. 16 from the tunnel face to the tunnel portal at the same times employing an airflow rate of 30 m^3 s^{-1}. The plug of toxic gases moves more slowly and the peak values of CO increase in the same times compared to the scenario that considers a higher airflow rate. Additionally, the distribution of the CO concentration 150 s after the start of the gas dilution process at different tunnel sections (75, 100, 125 and 150 m) is shown in Fig. 17 considering a ventilation volume of 40 m^3 s^{-1}. As previously indicated and presented in Figs. 12b and 13b, higher concentrations of CO are observed on the side of the tunnel in which the ducting system is located, requiring greater time for dilution. Note that Fig. 17d shows the top heading while the rest of Fig. represent the full section of the tunnel. The CO concentrations are illustrated in Fig. 18 in the same sections employing a ventilation volume of 30 m^3 s^{-1}. In general, higher levels of CO are observed in the sections when the airflow rate of 30 m^3 s^{-1} is used. Due to the greater ventilation volume, at the instant analyzed (t = 150 s) the gas plug does not reach section Z = 50 m using a flow of 30 m^3 s^{-1}, compared to the scenario that uses a higher airflow, in which a slight concentration of CO is obtained.

The results obtained considering a forced ventilation system have been compared with an exhaust ventilation system. In an exhaust ventilation system, the fresh air enters the tunnel, reaches the heading face and returns, together with the noxious gases, through the ventilation duct. The evolution of the CO concentration over time is shown in Fig. 19 after the blasting, considering the exhaust ventilation system. The toxic gases are concentrated only in the heading face area, not affecting other areas of the tunnel. The safe re-entry times increase compared to the forced system, reaching 765 and 1020 s using ventilation volumes of 40 and 30 m^3 s^{-1}, respectively.

3.2. Results of 1D model for gas dispersion

The results of the analytical model are shown in Fig. 20 to predict the re-entry times. Figs. 20a and b show the evolution of the CO concentrations at different sections employing ventilation volumes of 40 and 30 m^3 s^{-1}, respectively. The concentrations profiles for CO, NO and NO_2 exhibit a Gaussian-like distribution in the 1D analytical model, characterized by rapid growth and subsequent decline. In contrast, CFD simulations present a pattern of rapid growth followed by a slower decline in concentration. As obtained in the 3D CFD models, CO is the gas that needs the most time to dilute its concentration below the exposure limits established in the regulations. Re-entry times of 486 s and 649 s are obtained in the 1D model using flow rates of 40 and 30 m^3 s^{-1}, respectively, showing excellent agreements with the results of the 3D simulations.

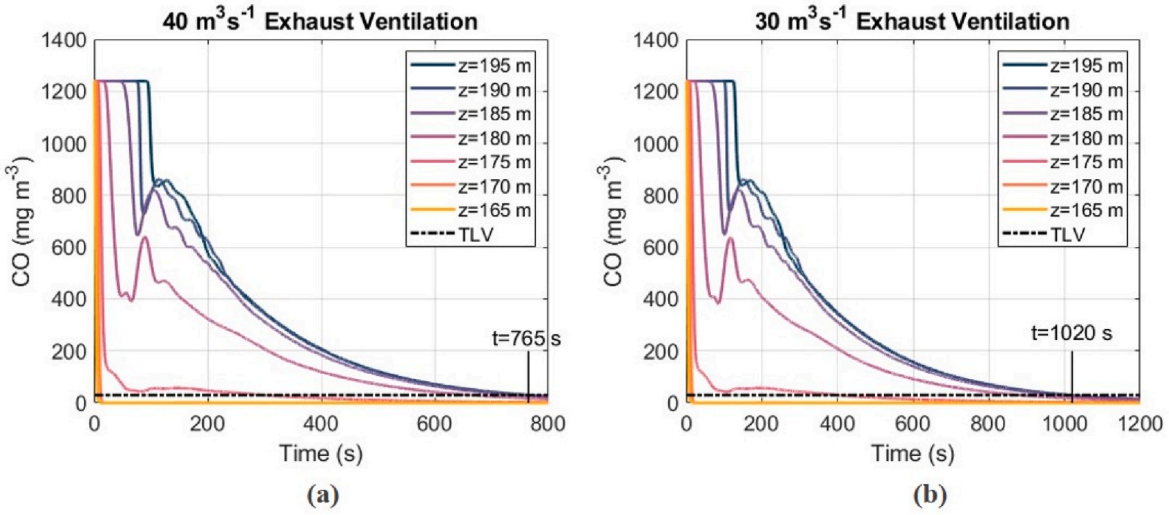

Fig. 19. CDF results. Exhaust ventilation mode. (a) Concentration-time curves of CO considering a ventilation volume of 40 m^3 s^{-1}; (b) Concentration-time curves of CO considering a ventilation volume of 30 m^3 s^{-1}.

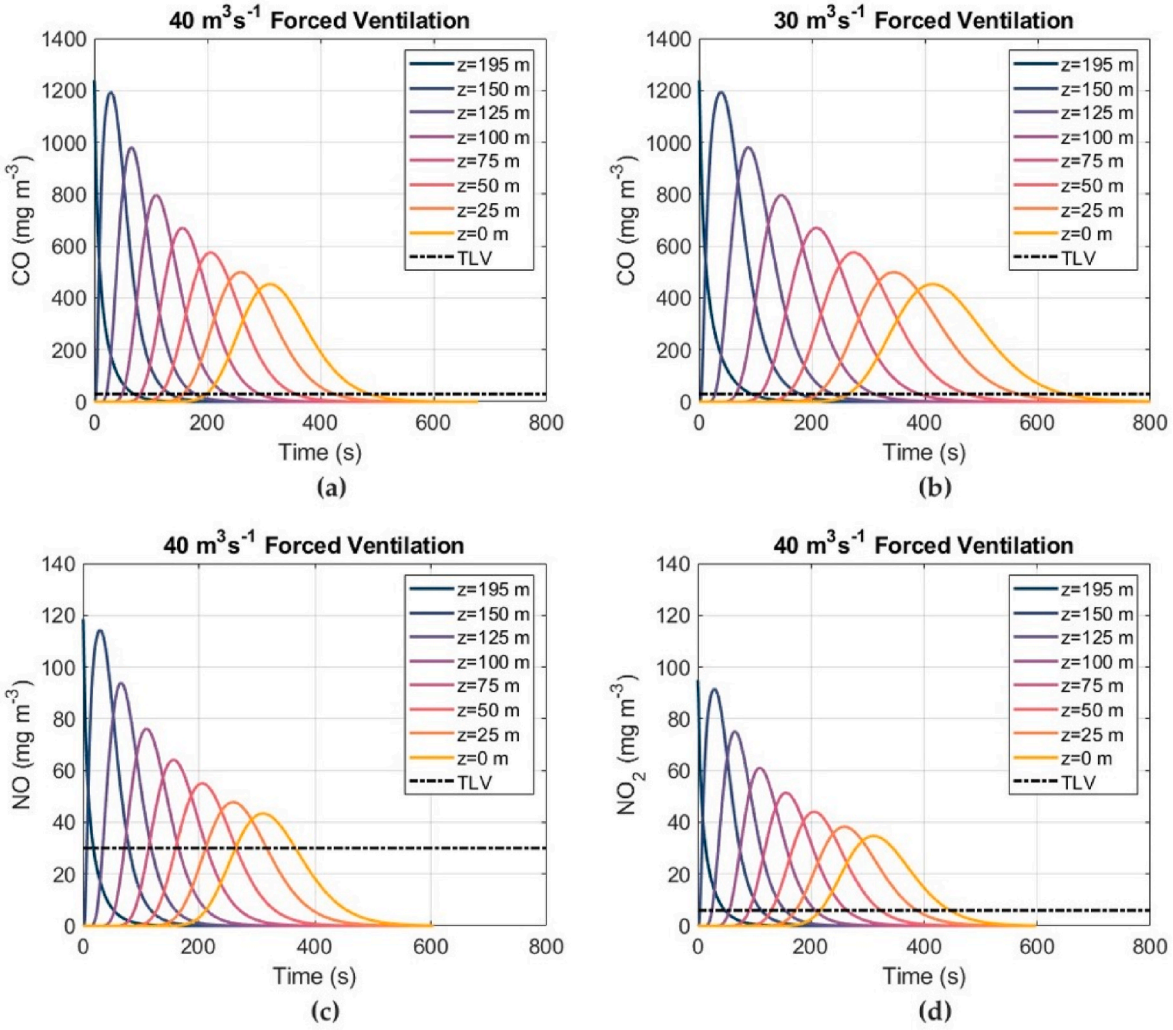

Fig. 20. 1D model results. Concentration-time curves of noxious gases at different sections along the tunnel. (a) Concentration of CO at 40 m^3 s^{-1}; (b) Concentration of CO at 30 m^3 s^{-1}; (c) Concentration of NO at 40 m^3 s^{-1}; (d) Concentration of NO_2 at 40 m^3 s^{-1}.

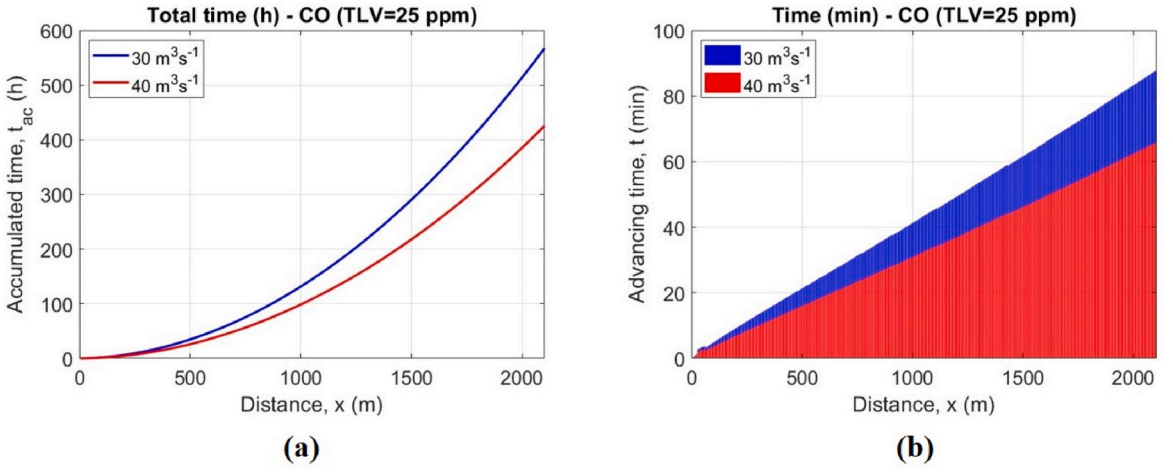

Fig. 21. Re-entry times at the work areas considering ventilation volumes of 30 and 40 m^3 s^{-1}. (a) Accumulated time for excavating the total length of the tunnel; (a) Re-entry time every advance cycle.

The safe re-entry times increase as tunnel excavation work progresses. Fig. 21b presents the re-entry times for every advance cycle considering typical tunnel advance rates of 5.4 m day^{-1} and ventilation volumes of 30 and 40 m^3 s^{-1}. As it concerns the critical gas, the time required to reduce CO concentrations has been taken into consideration. At the last advance cycle (2.1 km), the re-entry time reaches 83.8 min for

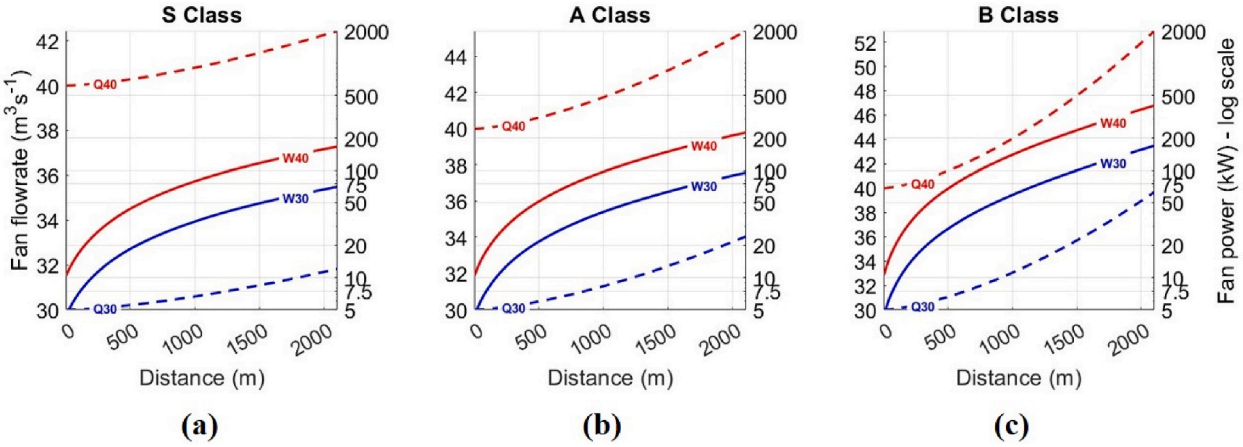

Fig. 22. Fan power and flow rate of leaks along the 1.8 m in diameter ducting system depending on the duct quality. (a) S Class; (b) A class; (c) B class.

Table 5
Air leaks along the ducting and fan power for 2.1 km long considering S, A and B ducting qualities.

Ducting Quality	Air leaks ($m^3\ s^{-1}$)		Fan power at 2.1 km long (kW)	
	30 $m^3\ s^{-1}$	40 $m^3\ s^{-1}$	30 $m^3\ s^{-1}$	40 $m^3\ s^{-1}$
S	1.8	2.4	70.6	166.7
A	4.1	5.4	95.2	225,8
B	9.6	12.9	170.1	403.2

30 $m^3\ s^{-1}$, decreasing down to 62.8 min when the airflow increases up to 40 $m^3\ s^{-1}$. The accumulated re-entry time required for the tunnel excavation is shown in Fig. 21a. The accumulated time for tunnel excavation reaches 552 and 414 h for airflow rates of 30 and 40 $m^3\ s^{-1}$, respectively.

3.3. Results of 1D model for air leakage and energy consumption

The ventilation volume varies along the ducting systems when leaky ducts are used in ventilation schemes. Depending on the ducting quality, a suitable design must be carried out to ensure the required ventilation volume at the work area. In addition, the fan power and the energy consumed by the ventilation system also depends on the duct class. Fig. 22 shows the fan power (solid lines) and the air leaks (dotted lines) along the 1.8 m in diameter ducting, considering the total excavation length with ventilation volumes of 30 and 40 $m^3\ s^{-1}$ and three ducting classes. According to the results presented in Table 5, the ventilation volume at the outlet of the fan for a B class ducting reaches 39.6 and 52.9 $m^3\ s^{-1}$ to provide air volumes at the tunnel face of 30 and 40 $m^3\ s^{-1}$, respectively. The fan power increases when the pressure inside the ducting system rises. Considering a B class duct for the total length of excavation, the power required by the fan reached 170.1 and 403.2 kW for airflow rates of 30 and 40 $m^3\ s^{-1}$, respectively. A typical fan efficiency of 75 % was considered. The power of the fan decreases significantly when the ducting condition improves.

Based on the results obtained in the fan power calculation, an analysis of the power required for each advance cycle has been conducted, regulating the fan power with the frequency converter. Considering daily advance cycles of 5.4 m, Fig. 23 illustrates the evolution of the consumed energy for the three ducting classes as the excavation length increases. Finally, the accumulated energy by the ventilation system for the tunnel excavation (2.1 km) is presented in Fig. 24. Considering a typical B class duct (Fig. 24c), the energy reaches 551.35 and 1,306.92 MWh with air volumes at the tunnel face of 30 and 40 $m^3\ s^{-1}$, respectively. When the ducting quality improves, the energy consumption decreases, reaching 278.60 and 660.39 MWh for 30 and 40 $m^3\ s^{-1}$, respectively, for a S class duct (Fig. 24a).

A balance between the re-entry times and the energy consumed by the ventilation system has been carried out. Table 6 shows the accumulated re-entry times and the energy consumption for the excavation of the total length of the tunnel using air volumes of 30 and 40 $m^3\ s^{-1}$ and three ducting qualities. The re-entry time increases by 33.4 % when the ventilation volume decreases from 40 to 30 $m^3\ s^{-1}$. However,

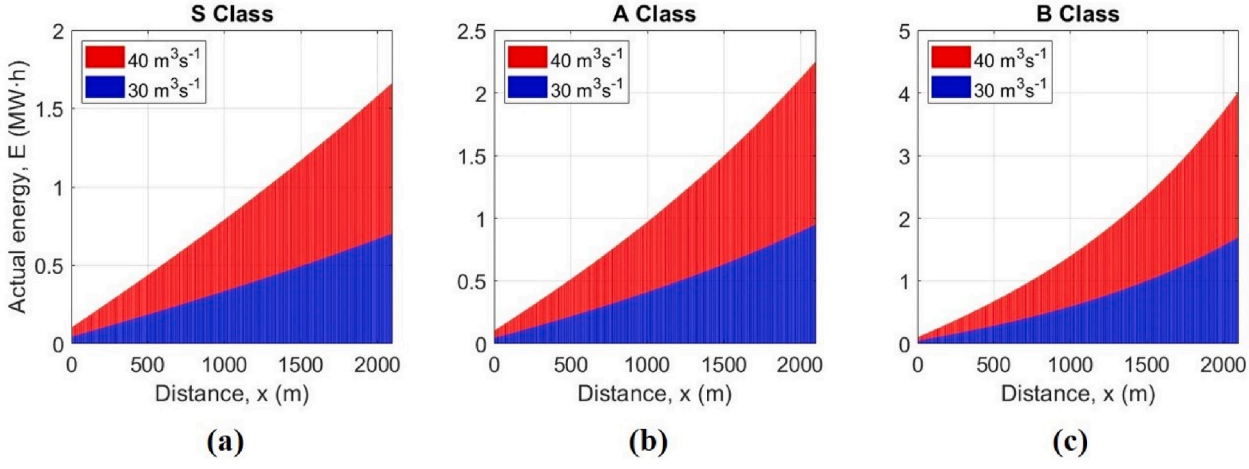

Fig. 23. Energy consumption along the tunnel excavation depending on the ducting class. (a) S Class; (b) A class; (c) B class.

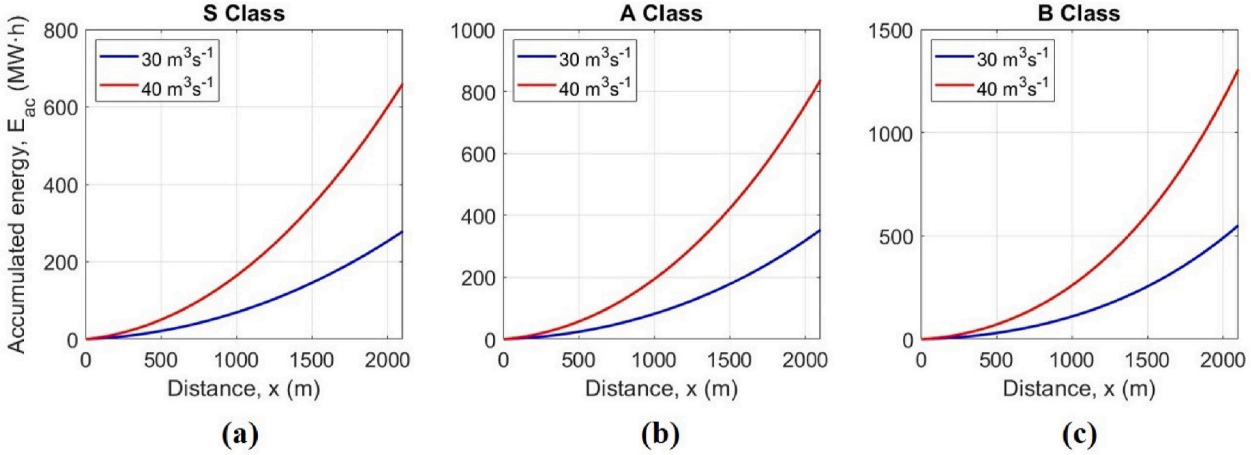

Fig. 24. Accumulated energy consumption by the ventilation system depending on the ducting class. (a) S Class; (b) A class; (c) B class.

Table 6
Accumulated re-entry times and energy consumption for the total excavation length.

Ducting Quality	Accumulated re-entry time (h)		Energy consumption (MWh)	
	30 m^3 s^{-1}	40 m^3 s^{-1}	30 m^3 s^{-1}	40 m^3 s^{-1}
S			278.60	660.39
A	552	414	353.26	837.36
B			551.35	1,306.92

considering a typical B class duct, the energy consumption increases from 551.35 to 1,306.92 MWh when the air volume increases up to 40 m^3 s^{-1}.

3.4. Analysis of optimal ventilation volume

The mathematical model that has been developed allows determining the optimal ventilation volumes at the heading face. The optimal ventilation volume is defined as that which results in the shortest re-entry time without causing an increase in ventilation costs. The safe re-entry time is reduced when the volume of fresh air increases. Based on the diesel power operating simultaneously in the tunnel and the number of workers, a minimum flow rate of 25 m^3 s^{-1} is required. The analysis of the optimal ventilation volumes is presented in Fig. 25 using S, A and B duct classes, considering airflow rates between 25 and 50 m^3 s^{-1}. Operating costs due to unproductive times after blasting (re-entry time costs) and ventilation costs are determined. An energy cost of 160 € MWh^{-1} and operation costs of 700 € h^{-1} are considered [42]. The re-entry time costs decrease as the ventilation volume increases, decreasing from 476.6 k€ to 238.3 k€ when the ventilation volume increases from 25 to 50 m^3 s^{-1} employing B class duct (Fig. 25c). Conversely, the ventilation costs increase from 51.0 k€ to 408.4 k€ when the airflow rate increases up to 50 m^3 s^{-1}. Therefore, optimal ventilation volumes of 39, 37 and 33 m^3 s^{-1} are obtained for S, A and B duct classes, respectively.

4. Conclusions

An assessment of the optimization of re-entry times after blasting operations in underground excavations is presented. A railway tunnel 2.1 km long under forced ventilation system has been selected as a case study to address productivity and safety concerns during the excavation works. 3D CFD numerical and 1D analytical models were conducted to predict re-entry times into the working areas considering a ducting system 1.8 m in diameter and different ventilation conditions. Field measurements were carried out to validate the precision of the results obtained in the simulations. Then, additional novel models were developed to evaluate the energy consumed by the ventilation system and the air leaks along the ducting system considering three different

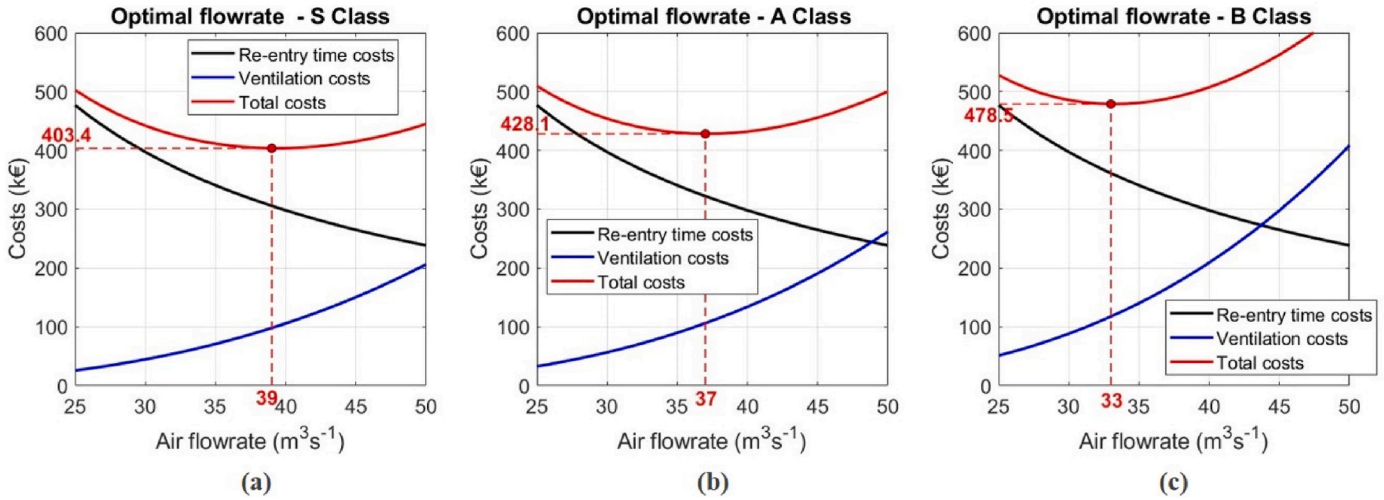

Fig. 25. Optimal air volume analysis considering re-entry time costs and ventilation costs. (a) S Class duct; (b) A class duct; (c) B class duct.

qualities (S, A and B) of the ducting system. Finally, a balance between the accumulated re-entry times and the energy consumption is carried out for the analyzed scenarios.

The results obtained show that longer dilution times are required for CO, compared to NO and NO_2. The accumulated re-entry time for the total excavation length reach 552 h using a ventilation volume at the work area of 30 $m^3 s^{-1}$. Re-entry times are reduced to 414 h when the airflow rate increases to 40 $m^3 s^{-1}$. Longer re-entry times are obtained using an exhaust ventilation mode. The energy consumed by the ventilation process depends strongly on the quality of the duct used. The energy consumed by the ventilation system reaches 551.35 MWh considering a typical B class duct and a ventilation volume of 30 $m^3 s^{-1}$. However, the energy consumption increases up to 1,306.92 MWh when the airflow rate increases to 40 $m^3 s^{-1}$. A significant reduction in energy consumption is obtained when the quality of the ventilation duct improves, reaching 660 MWh for a class S and an air volume of 40 $m^3 s^{-1}$.

Finally, optimal ventilation volumes were investigated considering airflow rates at the heading face between 25 and 50 $m^3 s^{-1}$. Operating costs due to unproductive times after blasting (re-entry time costs) and ventilation costs are compared employing different duct qualities. Optimal ventilation volumes of 39, 37 and 33 $m^3 s^{-1}$ are obtained for S, A and B duct classes, respectively.

CRediT authorship contribution statement

Javier Menéndez: Writing – review & editing, Writing – original draft, Visualization, Validation, Software, Methodology, Investigation, Conceptualization. **Mariano Sanabria:** Writing – review & editing, Writing – original draft, Visualization, Validation, Software, Methodology, Investigation. **Jesús Manuel Fernández-Oro:** Writing – review & editing, Writing – original draft, Visualization, Validation, Software, Investigation. **Mónica Galdo-Vega:** Software, Investigation. **Laura Álvarez de Prado:** Validation, Methodology, Investigation, Conceptualization. **Antonio Bernardo-Sánchez:** Validation, Supervision, Investigation, Conceptualization.

Declaration of competing interest

The authors declare that they have no known competing financial interests or personal relationships that could have appeared to influence the work reported in this paper.

Data availability

Data will be made available on request.

References

[1] Mainiero RJ, Harris ML, Rowland JH. Dangers of toxic fumes from blasting. International society of explosives engineers (ISEE). In: Proceedings of the 33rd annual conference on explosives and blasting technique; 2007. p. 1–6. January 28 - 31, 2007, Nashville, USA.

[2] OSHA permissible exposure limits, OSHA annotated table Z-1. https://www.osha.gov/dsg/annotated-pels/table-z-1.html. [Accessed 23 February 2022].

[3] Huang R, Shen X, Wang B, Liao XP. Migration characteristics of CO under forced ventilation after excavation roadway blasting: a case study in a plateau mine. J Clean Prod 2020;267:122094.

[4] Bahrami D, Yuan L, Rowland JH, Zhou L, Thomas R. Evaluation of postblast re-entry times based on gas monitoring of return air. Min. Metall. Explor. 2019;36:513–21.

[5] Torno S, Toraño J, Ulecia M, Allende C. Conventional and numerical models of blasting gas behaviour in auxiliary ventilation of mining headings. Tunn Undergr Space Technol 2013;34:73–81.

[6] Feng Xue, Jiang Zhongan, Zhang Guoliang, Luo Xun, Zeng Fabin. Study on CO diffusion law and concentration distribution function under ventilation after blasting in high-altitude tunnel. J Wind Eng Ind Aerod 2022;220:104871.

[7] Torno S, Toraño J. On the prediction of toxic fumes from underground blasting operations and dilution ventilation. Conventional and numerical models. Tunn Undergr Space Technol 2020;96:103194.

[8] Pu QS, Luo Y, Huang JH, Zhu YW, Hu SH, Pei CH, Zhang G, Li XP. Simulation study on the effect of forced ventilation in tunnel under single-head drilling and blasting. Shock Vib 2020;2020:8857947.

[9] Huang L, Bohne RA, Bruland A, Jakobsen PD, Lohne J. Environmental impact of drill and blast tunnelling: life cycle assessment. J Clean Prod 2015;86:110–7.

[10] De Souza EM, Katsabanis P. On the prediction of blasting toxic fumes and dilution ventilation. Min Sci Technol 1991;13(2):223–35.

[11] Stewart CM. Practical prediction of blast fume clearance and workplace re-entry times in development headings. In: Proceedings of the 10th international mine ventilation congress, Sun City; August 2014. p. 2–8. South Africa.

[12] Agson Gani PH, Widodo NP, Sitorus T. Study of re-entry time post blasting at ciguha PT ANTAM UBPE pongkor underground gold mine. In: 17th North American mine ventilation symposium (NAMVS 2019); 2019 (Montreal, Canada).

[13] Sirait SH, Widodo NP, Simanjuntak M. Study on estimation of re-entry time after blasting in underground mining PT Cibaliung Sumberdaya, Indonesia. In: Proceedings of international symposium on earth science and technology; 2013. 3-4 December, 2013, Fukuoka, Japan.

[14] Gillies A, Wu H, Shires D. Development of an assessment tool to minimize safe after blast re-entry time to improve the mining cycle. In: Proceedings of the tenth US/North American mine ventilation Sm; 2004. p. 315–24. Alaska, USA.

[15] Harris ML, Mainiero RJ. Monitoring and removal of CO in blasting operations. Saf Sci 2008;46:1393–405.

[16] Harris ML, Sapko MJ, Mainiero RJ. Field studies of CO migration from blasting. In: Proceedings of the 31st annual conference on explosives and blasting technique, vol. II. Cleveland, OH: International Society of Explosives Engineers; 2005. p. 49–69. February 6-9.

[17] Lawrence, D. L. (1995). A study of post blast generation of nitrogen dioxide. Proceedings of the 22nd annual conference on explosives and blasting technique. February 2-5 (pp 1-12) Cleveland, OH: International Society of Explosives Engineers.

[18] Mayala LP, Veiga MM, Khorzoughi MB. Assessment of mine ventilation systems and air pollution impacts on artisanal tanzanite miners at Merelani, Tanzania. J Clean Prod 2016;116:118–24.

[19] Fang Y, Yao Z, Lei S. Air flow and gas dispersion in the forced ventilation of a road tunnel during construction. Tunn Undergr Space Technol 2019;4:168–79.

[20] Li M, Aminossadati SM, Wu C. Numerical simulation of air ventilation in super-large underground developments. Tunn Undergr Space Technol 2016;52:38–43.

[21] Zhang Y, Xie Y, Lai J, Li Y. Distribution of harmful gas concentration of plateau tunnel under the forced ventilation mode. J Railw Sci Eng 2016;13:1994–2000.

[22] Zou ZL, Hu XB, Yuan Y, Chen JZ. Monitoring study on CO and dust diffusion in high altitude tunnel under blasting operation. IOP Conf Ser Mater Sci Eng 2020;741(1).

[23] Cao Z, Yang Q, Guo C. Migration characteristics of poisonous gas during construction stage in railway tunnels at high altitude areas. J. Cent. South Univ. (Nat. Sci.) 2016;47:3948–57.

[24] Chang XK, Chai JR, Luo JP, Qin Y, Xu ZG, Cao J. Tunnel ventilation during construction and diffusion of hazardous gases studied by numerical simulations. Build Environ 2020;177:106902.

[25] Xin S, Wang WH, Zhang NN, et al. Comparative studies on control of thermal environment in development headings using force/exhaust overlap ventilation systems. J Build Eng 2021;38:10222.

[26] Bubbico R, Mazzarotta B, Verdone N. CFD analysis of the dispersion of toxic materials in road tunnels. J Loss Prev Process Ind 2014;28:47–59.

[27] Liu Q, Nie W, Hua Y, Peng HT, Ma H, Yin S, Guo LD. Long-duct forced and short-duct exhaust ventilation system in tunnels: formation and dust control analysis of pressure ventilation air curtain. Process Saf Environ Protect 2019;132:367–77.

[28] Jiang ZA, Wang YP, Men LG. Ventilation control of tunnel drilling dust based on numerical simulation. J. Cent. South Univ. 2021;28:1342–56.

[29] Agasty A, Clausen E, Kellner M, Langefeld O. After blast re-entry time for a room and pillar operation. In: Proceedings the Australian mine ventilation conference; 2013. p. 179–86.

[30] Roman WN, Guthrie J, Ndhlovu W. Upgrading ventilation systems at Konkola mine, Zambia. In: Proceedings of the North American/ninth US mine ventilation symposium. Canada: Kingston; 2002. p. 8–12. June 2002.

[31] Adhikari A, Jayaraman S, Tukkaraja P, Sasmito A, Vytla S. The effect of trapped fumes on clearance time in underground development blasting. Min. Metall. Explor. 2022;39:1811–20.

[32] De Souza E, Katsabanis P, Roberts W, Heidrich H. Blasting fume prediction and control as a means of reducing ventilation costs. In: Proceedings of the 6th US mine ventilation symposium: June 21–23, 1993. of Utah, Salt Lake City, Utah: University; 1993.

[33] Nie W, Jiang S, Liu Q, Guo L, Hua Y, Zhang H, Jiang B, Zhu Z. Study of highly efficient control and dust removal system for double-tunnel boring processes in coal mines. Energy 2024;289:130081.

[34] Lu X, Wang CV, Shen C, Wang M, Xing Y. Verisimilar research on the dust movement in the underground tunneling at the roadheader cutterhead dynamic rotation. Energy 2022;238:121978.

[35] Xie Z, Zhao Z, Li D, Jiang T, Wang T, Xiao Y. Field measurements on the attenuation characteristics of PM2.5 and toxic gases in a blasting metro tunnel and evaluation of the re-entry time. Tunn Undergr Space Technol 2023;138:105170.

[36] Zhang G. Ventilation safety. second ed. Xuzhou: China University Mining Technology Press; 2011.

[37] Rowland III, J H, Mainiero R, Hurd Jr DA. Factors affecting fumes production of an emulsion and ANFO/emulsion blends. Proc. In: 27th annual conference on explosives and blasting technique, Orlando, USA 28-31 jan. 2001. p. 133–41.

[38] Brake DJ. A review of good practice standards and re-entry procedures after blasting and gas detection generally in underground Hardrock mines. In: 15th North American mine ventilation symposium; 2015. p. 20–5. Blacksburg. Virginia, June, 21-23.
[39] Menéndez J, Merle N, Fernández-Oro JM, Galdo M, Álvarez L, Loredo J, Bernardo-Sánchez A. Concentration, propagation and dilution of toxic gases in underground excavations under different ventilation modes. Int J Environ Res Publ Health 2022; 19:7092.
[40] Moen A, Mauri L, Narasimhamurthy VD. Comparison of k-ε models in gaseous release and dispersion simulations using the CFD code FLACS. Process Saf. Environ. 2019;130:306–16.
[41] Hákonardóttir KM, Tómasson G, Kaelin J, Stefánsson B. The hydraulic roughness of unlined and shotcreted TBM-bored tunnels in volcanic rock: in situ observations and measurements at Kárahnjúkar Iceland. Tunn Undergr Space Technol 2009;24 (6):706–15.
[42] Menéndez J, Fernández-Oro JM, Merle N, Galdo M, Álvarez L, López-Fanjul C, Bernardo-Sánchez A. Auxiliary ventilation systems in tunnelling and mining. Air leakage prediction and system design to optimize the energy efficiency and operation costs Tunn. Undergr. Space Technol. 2023;140:105298.
[43] SIA 196 - Recommendation - Edition. Ventilation in underground construction, Swiss engineering and architects association. 1998.